Title

Strain Tuning in Complex Oxide Epitaxial Films Using an Ultrathin Strontium Aluminate Buffer Layer

Di Lu, Yasuyuki Hikita, David J. Baek, Tyler A. Merz, Hiroki Sato, Bongju Kim, Takeaki Yajima, Christopher Bell, Arturas Vailionis, Lena F. Kourkoutis, Harold Y. Hwang*

D. Lu
Department of Physics, Stanford University, Stanford, California 94305, USA
E-mail: dilu@stanford.edu
Dr. Y. Hikita, Dr. H. Sato, Dr. T. Yajima, Dr. C. Bell, Prof. H. Y. Hwang
Stanford Institute for Materials and Energy Sciences, SLAC National Accelerator Laboratory, Menlo Park, California, 94025, USA
D. J. Baek
School of Electrical and Computer Engineering, Cornell University, Ithaca, New York, 14853, USA
T. A. Merz, Dr. B. Kim, Prof. H. Y. Hwang
Department of Applied Physics Stanford University, Stanford, CA, 94305, USA
Dr. H. Sato
Department of Advanced Materials Science, The University of Tokyo, Kashiwa, Chiba, 277-8561, Japan
Dr. T. Yajima
Department of Materials Engineering, The University of Tokyo, Bunkyo, Tokyo, 113-8656, Japan
Dr. C. Bell
H. H. Wills Physics Laboratory, University of Bristol, Tyndall Avenue, Bristol, BS8 1TL, UK
Dr. A. Vailionis
Stanford Nano Shared Facilities, Stanford University, Stanford California, 94305, USA
Prof. L. F. Kourkoutis
School of Applied and Engineering Physics, Cornell University, Ithaca, New York, 14853, USA & Kavli Institute at Cornell for Nanoscale Science, Cornell University, Ithaca, New York, 14853, USA

Keywords: oxides, epitaxy, strain control, ultrathin buffer layers, relaxation

Abstract

A reliable method to apply biaxial strain over a wide range of values with minimal dislocation generation is critical for the study of strain dependent physical properties in oxide thin films and heterostructures. In this work, we systematically controlled the strain state in a perovskite manganite thin film by as much as 1 % using a new ultrathin strain-releasing buffer layer $Sr_3Al_2O_6$, and observed signatures of accompanying magnetic and metal-insulator transitions. The near-zero strain state was achieved within 5 nanometers of buffer layer thickness, substantially thinner than

any oxide epitaxial buffer layers that can continuously tune the film strain states. Furthermore, the majority of misfit dislocations were confined to the $Sr_3Al_2O_6$ layer, structurally decoupling defects in the film from the substrate.

Epitaxial strain is one of the most effective parameters for controlling the physical properties in complex oxide thin films and heterostructures given their sensitivity to metal-oxygen bonding length and bonding angles.[1] The static lattice constant mismatch between a substrate and a film can reach as much as several percent, sufficient to induce significant modification of the film electronic structure as demonstrated by changes in the phase transition temperature in superconducting cuprates, ferroelectric titanates, and colossal magnetoresistive manganites.[2-4] Further strain tuning in the dynamic regime has also been enabled by employing piezoelectric templates.[5] Despite much success, the use of different substrates[4,6,7] generally suffers from variation in the type and density of dislocations in the film, potentially leading to different film crystalline quality. In order to mitigate such substrate specific effects, growth of epitaxial thin films on a strain-relaxing buffer layer has been suggested as an effective approach to systematically control the strain over a wide range.[8] These buffer layers are typically isostructural to the film and the substrate (e.g. perovskite layers on perovskite substrate), and the high stiffness of oxides inevitably requires large buffer thicknesses (~ few hundred nm per 1 % strain) to fully relax the film,[9,10] increasing the probability of dislocations propagating through the film.[11] Here we report that by using a new strain-relaxing oxide buffer layer $Sr_3Al_2O_6$ (strontium aluminate), we successfully controlled the strain state up to

1 % (measured by in-plane lattice constant change) in a perovskite manganite film on a (001)-oriented $SrTiO_3$ substrate within 5 nm of the buffer layer, while preserving the high-quality of the perovskite oxide films allowing systematic modulation of their electronic and magnetic properties.

The highly efficient strain-relaxing properties of $Sr_3Al_2O_6$ arise from its characteristic crystal structure (space group $Pa\bar{3}$). Unlike the cubic perovskites (space group $Pm\bar{3}m$) in which the corner-shared octahedra are interconnected three-dimensionally, the tetrahedrally-coordinated AlO_4 clusters form independent 12-membered $(Al_6O_{18})^{18-}$ rings, which are separated by Sr atoms in $Sr_3Al_2O_6$.[12] The large radii of the $(Al_6O_{18})^{18-}$ clusters and Sr^{2+} ions increase the distance between the charges, and therefore, weaken the Coulomb interaction between them, making the estimated elastic moduli of $Sr_3Al_2O_6$ smaller by 50 to 60 % compared to typical perovskites such as $SrTiO_3$.[13, 14] Either the elastic deformation from the small Young's modulus or the formation of dislocations due to the small shear modulus[15] allows $Sr_3Al_2O_6$ to absorb a large lattice mismatch within short length scales. While its elastic properties differ greatly from those of perovskites, the surprisingly similar atomic positions and the small lattice mismatch enable high quality epitaxial growth of $Sr_3Al_2O_6$ thin films on perovskite substrates. Namely, $Sr_3Al_2O_6$ has a cubic unit cell with lattice constant a = 15.844 Å, corresponding to 101.4 % of four $SrTiO_3$ unit cells (4×3.905 = 15.620 Å) and the atomic positions on the perovskite (001) plane can be directly projected onto the $Sr_3Al_2O_6$ (001) plane.[12]

To examine the strain relaxation properties of $Sr_3Al_2O_6$, we grew thin films of $Nd_{0.5}Sr_{0.5}MnO_3$ as a model system due to its dramatic strain-dependent phase transition at low temperatures. Bulk $Nd_{0.5}Sr_{0.5}MnO_3$ undergoes a paramagnetic metal (PM) to a ferromagnetic metal (FM) transition at 270 K, which further transitions into a charge-ordered antiferromagnetic (CO-AFM) insulator

below $T_{CO,bulk}$ = 150 K.[16,17] The FM/CO-AFM transition at $T_{CO,bulk}$ is accompanied by a structural phase transition involving anisotropic expansion of the orthorhombic lattice. The FM phase possesses *Pbnm* symmetry (*a* = 5.4726 Å, *b* = 5.4264 Å, *c* = 7.6240 Å) with three rotated axes of the MnO_6 octahedra, which transitions into the CO-AFM state with *Ibmm* symmetry (*a* = 5.5114 Å, *b* = 5.4400 Å, *c* = 7.5180 Å) with quadrupled in-plane unit cell hosting two rotations in the MnO_6 octahedra.[16] Given the small differences from the cubic perovskite structure, we use the approximate pseudo-cubic lattice notation to represent the structural phase transition, in which $a' = a/\sqrt{2}$, $b' = b/\sqrt{2}$ and *c'=c/2*. In this notation, the FM/CO-AFM transition is a pseudo-cubic FM (*a'* ≈ *b'* ≈ *c'*) to a pseudo-tetragonal CO (*a'* ≈ *b'* > *c'*) lattice. Here, *a'* and *b'* are the in-plane and *c'* is the out-of-plane lattice constants with respect to the film surface.

The strong coupling of lattice symmetry and charge/magnetic order is more pronounced in epitaxial thin films. Without buffer layers, for example, strained $Nd_{0.5}Sr_{0.5}MnO_3$ films on a $SrTiO_3$ (001) substrate only exhibits the CO-AFM state below 270 K, suppressing the FM state found in bulk due to the tensile in-plane strain stabilizing the pseudo-tetragonal phase.[18-20] The bulk-like FM/CO-AFM transition can be recovered by growth on (110)-oriented $SrTiO_3$ substrate due to the anisotropic strain allowing access to both the pseudo-cubic and the pseudo-tetragonal lattices by a shear deformation of the lattice (**Figure S1**).[18,21,22] This sensitivity of the FM/CO transition provides a useful signature to probe the subtle changes in the strain state of the film induced by the $Sr_3Al_2O_6$ buffer layer in (001)-oriented films; by gradually relaxing the in-plane lattice constant in $Nd_{0.5}Sr_{0.5}MnO_3$ films from the substrate, an evolution of the FM/CO-AFM transition is expected.

To fabricate the samples, TiO_2-terminated $SrTiO_3$ (001) substrates were pre-annealed at 950 °C under oxygen partial pressure $p(O_2)$ of 5.0×10^{-6} Torr for 30 min to achieve smooth, single terminated step and terrace surfaces. The $Sr_3Al_2O_6$ buffer layers and the $Nd_{0.5}Sr_{0.5}MnO_3$ films were

grown on these $SrTiO_3$ (001) substrates sequentially using a 248-nm KrF excimer laser. $Sr_3Al_2O_6$ and $Nd_{0.5}Sr_{0.5}MnO_3$ targets were used for the respective film growth. $Sr_3Al_2O_6$ was grown at a substrate temperature T_g = 700 °C and $p(O_2) = 1.0 \times 10^{-5}$ Torr, using 1.25 J/cm^2 laser fluence and 4 mm^2 spot size. $Nd_{0.5}Sr_{0.5}MnO_3$ was grown at T_g = 825 °C and $p(O_2) = 2.0 \times 10^{-3}$ Torr, using 0.40 J/cm^2 laser fluence and 11 mm^2 spot size. The latter conditions were carefully chosen to achieve the nominal cation stoichiometry in the $Nd_{0.5}Sr_{0.5}MnO_3$ films: **Figure S2** shows the transport and magnetic properties of a $Nd_{0.5}Sr_{0.5}MnO_3$ film on $SrTiO_3$ (110) substrate clearly reproducing the two phase transitions previously reported.[18] These data indicate that the systematic behavior observed in our strain-controlled $Nd_{0.5}Sr_{0.5}MnO_3$ films does not arise from cation off-stoichiometry.[16] During sample growth, reflection high-energy electron diffraction (RHEED) was used to monitor the sample quality and thickness.

Various methods are used to characterize the samples. The scanning transmission electron microscopy (STEM) images were measured using a 200 keV FEI Tecnai F20 SuperTWIN STEM. The reciprocal space mapping data in Figure 1b, c were measured using a laboratory source Cu-$K_{\alpha 1}$ X-ray diffraction (XRD) equipped with a monochromator. The transport measurement was carried out using the four-probe method in a liquid helium cryostat and the magnetic properties were measured using a superconducting quantum interference device magnetometer with a field of 100 Oe applied parallel to the in-plane direction of the film. The temperature dependent XRD measurements were taken at BL7-2 at Stanford Synchrotron Radiation Lightsource, SLAC National Accelerator Laboratory using a four-axis diffractometer equipped with a cryostat.

We grew 80 nm-thick $Nd_{0.5}Sr_{0.5}MnO_3$ films on $SrTiO_3$ (001) substrates with x nm-thick (x = 0, 2.4, 3.6, 4.8) $Sr_3Al_2O_6$ buffer layers inserted by pulsed laser deposition (PLD).[23] Layer-by-layer growth of $Nd_{0.5}Sr_{0.5}MnO_3$ was detected by RHEED intensity modulations (**Figure 1a**). The

$Nd_{0.5}Sr_{0.5}MnO_3$ film is strained to the substrate for x = 0 and gradually relaxed to its bulk values at x = 4.8 as confirmed by high-resolution room temperature XRD (**Figure 1b, c, Figure S3**).

We observed micrometer-scale lateral uniformity in the crystallinity with minimum dislocation density by using STEM as shown for x = 4.8 in **Figure 2a, b**. From the low angle annular dark field (LAADF) image in **Figure 2c**, which highlights the strain field in the specimen,[24] an approximately 2 nm thick clear high-strain region at the $Sr_3Al_2O_6/SrTiO_3$ interface is seen, suggesting that the strain is mainly confined there. No such high-strain band at the top $Nd_{0.5}Sr_{0.5}MnO_3/Sr_3Al_2O_6$ interface was observed. The dislocations in the $Sr_3Al_2O_6$ layer next to the high-strain region (**Figure 2d**) appeared with a periodicity of approximately 50 nm, roughly matching the dislocation density calculated to compensate the ~ 1 % in-plane lattice relaxation of $Nd_{0.5}Sr_{0.5}MnO_3$ (001) from 3.889 Å to 3.851 Å (Figure 1c). This evidence of domain matching epitaxy[25] strongly supports the picture of strain relaxation through formation of periodical dislocations in the $Sr_3Al_2O_6$ as thin as 4.8 nm and confirms the structural decoupling of the defects in $Nd_{0.5}Sr_{0.5}MnO_3$ from $SrTiO_3$.

The evolution of the film physical properties in controlled strain states were probed by crystal structure, electronic transport and magnetization measurements. For x = 0 and 2.4, the in-plane lattice constant and tetragonality (pseudo-cubic a'/c') measurements from temperature dependent XRD (**Figure 3a**) indicate no structural phase transition down to T = 60 K. The high tetragonality (a'/c' ~ 1.03), together with their insulating behavior and small magnetization (**Figure 3b, c**) indicate that these films are in the CO phase below 270 K.

By contrast, the x = 3.6 sample shows an in-plane lattice expansion at T_{film} ~ 170 K (Figure 3a), similar to the increase of the a'/c' ratio across the FM/CO transition at $T_{CO,bulk}$ ~ 150 K in bulk. The broad metal-insulator transition in transport, and a kink in the magnetization curve both at 170 K

with clear hysteresis (Figure 3b, c) suggest that the transition at T_{film} ~ 170 K is the FM/CO-AFM transition. To further verify the presence of a FM/CO-AFM phase transition below T_{film} for x = 3.6, we measured the temperature evolution of the charge-ordered superlattice diffraction peaks.[26,27] Bulk $Nd_{0.5}Sr_{0.5}MnO_3$ is believed to exhibit a planar checkerboard charge ordering pattern with alternating Mn^{3+} and Mn^{4+} ions with a nesting vector parallel to [1/4 1/4 0].[26] By linearly scanning along the film pseudo-cubic reciprocal space (1/4 1/4 3+L), we observed a peak at around (1/4 1/4 3.03) at temperatures below T_{film}, which diminishes rapidly above this transition temperature (**Figure 4a**). Moreover, the HK-scan around (1/4+H 1/4+K 3.03) showed that the (1/4 1/4 3.03) charge ordering peak at low temperatures disappears at higher temperatures (**Figure 4b, c**), indicating the emergence of a quadrupled in-plane unit cell accompanied by a long-range out-of-plane modulation.

The $Nd_{0.5}Sr_{0.5}MnO_3$ film which was almost fully relaxed to its bulk lattice constants at room temperature (x = 4.8) unexpectedly did not recover the full bulk properties. Temperature dependent XRD measurement showed no sign of a structural phase transition in the film (Figure 3a). Similarly, no sign of the FM/CO-AFM transition was obtained from transport or magnetization measurements and the film remained in the FM state below 270 K (Figure 3b, c). To understand the behavior of the x = 4.8 film requires clarification of the key factors governing the $Nd_{0.5}Sr_{0.5}MnO_3$ FM/CO-AFM transition. To achieve a bulk-like phase transition, the film lattice must be able to transform into both the pseudo-cubic and pseudo-tetragonal structures via bi-axial stress or shear deformation (Figure S1). For all the (001)-oriented films studied in this work, the latter structure is suppressed by symmetry, therefore the tolerable lattice constant variation due to bi-axial stress mainly determines the realization of the FM/CO-AFM transition. For the $Nd_{0.5}Sr_{0.5}MnO_3$ films grown on the buffer layers, we believe that their tetragonality is able to change within a small range, due to

the weaker mechanical properties of $Sr_3Al_2O_6$ compared with typical perovskite oxides.[13,14] As a result, if the as-grown in-plane film lattice constant is within the variable range of the CO-AFM phase lattice constant, signatures of the FM/CO-AFM phase transition will appear as in the case of x = 3.6. However, if the as-grown in-plane lattice constant is far from either the FM phase or the CO-AFM phase, the lattice constant cannot change sufficiently to reach the other phase and the phase transition is suppressed, maintaining the as-grown phase down to the lowest temperatures, which appears to be the case for x = 2.4 and 4.8.

We note that the x = 4.8 film exhibited two peaks in XRD (Figure 3a and Figure S3), which we attribute to a fully relaxed state, as well as a section of the film under ~ 0.15% tensile strain judging from their peak positions. In agreement to the observation from XRD for the x = 4.8 film, we observe the presence of two different regions along the film's growth direction that is separated by a horizontal region of dark contrast as illustrated in the magnified HAADF-STEM image in **Figure S4**. We speculate that in addition to the major interfacial dislocations, the substantially smaller strain state of the x = 4.8 film tends to kinetically trap the dislocations within the film, instead of migrating into the buffer layer and hence the absence of multiple peaks in other films (x = 0, 2.4, and 3.6).[28]

The $Sr_3Al_2O_6$ buffer readily provides opportunities to investigate the properties of perovskite oxide films in different strain states. For example, other representative perovskites such as $SrTiO_3$, $La_{0.7}Sr_{0.3}MnO_3$, and their superlattices have been stabilized on $Sr_3Al_2O_6$.[23] We also have successfully grown strain controlled $Nd_{0.5}Sr_{0.5}MnO_3$ 80 nm / $Sr_3Al_2O_6$ 4.8 nm on a $LaSrAlO_4$ (a = 3.756 Å) substrate as shown in **Figure S5**, demonstrating the ability of $Sr_3Al_2O_6$ to accommodate an in-plane lattice mismatch over a range of -1.34 % (on $SrTiO_3$) to +2.53 % (on $LaSrAlO_4$) within a thickness of a few nanometers. Furthermore, the buffer layer lattice constant varies in accordance

with Vegard's law by substituting Ca or Ba for Sr in $Sr_3Al_2O_6$ which allows the precise control of the strain state to further reduce the dislocation density (**Figure S6**). No depth-dependent relaxation is observed in this case due to the negligible lattice mismatch between the Ca:$Sr_3Al_2O_6$ and the $Nd_{0.5}Sr_{0.5}MnO_3$ film.

In summary, we demonstrated the utility of $Sr_3Al_2O_6$ as a highly-efficient strain-tuning oxide buffer layer in the $Nd_{0.5}Sr_{0.5}MnO_3$ / $SrTiO_3$ (001) system. The 1.34 % in-plane lattice mismatch was almost fully relaxed within 5 nm of buffer thickness substantially thinner than previous oxide epitaxial buffer layers.[8-10] The misfit dislocations were predominantly confined to the buffer layer. Tunable magnetic and transport properties of $Nd_{0.5}Sr_{0.5}MnO_3$ thin films were also observed by controlling their strain states. By applying this method to other oxide films or heterostructures, the $Sr_3Al_2O_6$ buffer layer method can be a general solution to reliably enhance their designated physical properties, especially the unique properties in oxides such as high T_c superconductivity, ferroicity and ordering of charge, orbital and spin, by controlling their strain states.

Supporting Information

Supporting Information is available from the Wiley Online Library.

Acknowledgements

This work is supported by the Department of Energy, Office of Basic Energy Sciences, Division of Materials Sciences and Engineering, under contract DE-AC02-76SF00515. D. L. also acknowledges partial support from Gordon and Betty Moore Foundation's EPiQS Initiative through Grant GBMF4415. T. A. M. also acknowledges support from the National Science Foundation Graduate Research Fellowship under Grant No. DGE-114747. Work at Cornell (D.B., L.F.K.) was supported by the Cornell Center for Materials Research with funding from the NSF MRSEC program (DMR-1120296). Use of the Stanford Synchrotron Radiation Lightsource, SLAC National Accelerator Laboratory, is supported by the U.S. Department of Energy, Office of Science, Office of Basic Energy Sciences under Contract No. DE-AC02-76SF00515.

Received: ((will be filled in by the editorial staff))
Revised: ((will be filled in by the editorial staff))
Published online: ((will be filled in by the editorial staff))

[1] A. Imada, A. Fujimori, Y. Tokura, *Rev. Mod. Phys.* **1998**, *70*, 1039.

[2] J. P. Locquet, J. Perret, J. Fompeyrine, E. Machler, J. W. Seo, G. Van Tendeloo, *Nature* **1998**, *394*, 453.

[3] J. H. Haeni, P. Irvin, W. Chang, R. Uecker, P. Reiche, Y. L. Li, S. Choudhury, W. Tian, M. E. Hawley, B. Craigo, A. K. Tagantsev, X. Q. Pan, S. K. Streiffer, L. Q. Chen, S. W. Kirchoefer, J. Levy, D. G. Schlom, *Nature* **2004,** *430*, 758.

[4] F. Tsui, M. C. Smoak, T. K. Nath, C. B. Eom, *Appl. Phys. Lett.* **2000**, *76*, 2421.

[5] C. Thiele, K. Dörr, S. Fähler, L. Schultz, D. C. Meyer, A. A. Levin, P. Paufler, *Appl. Phys. Lett.* **2005**, *87*, 262502.

[6] D. G. Schlom, L.-Q. Chen, C.-B. Eom, K. M. Rabe, S. K. Streiffer, J.-M. Triscone, *Annu. Rev. Mater. Res.* **2007**, *37*, 589.

[7] M.-W. Chu, I. Szafraniak, R. Scholz, C. Harnagea, D. Hesse, M. Alexe, U. Gösele, *Nature Mater.* **2004**, *3*, 87.

[8] W. D. Si, X. X. Xi, *Appl. Phys. Lett.* **2001**, *78*, 240.

[9] J. W. Matthews, A. E. Blakeslee, *J. Cryst. Growth* **1974**, *27*, 118.

[10] L. B. Freund, W. D. Nix, *Appl. Phys. Lett.* **1996**, *69*, 173.

[11] J. Tersoff, *Appl. Phys. Lett.* **1993**, *62*, 693.

[12] J. A. Alonso, I. Rasines, J. L. Soubeyroux, *Inorg. Chem.* **1990**, *29*, 4768.

[13] L.-G. Hwa, G.-W. Lee, *Mater. Chem. Phys.* **1999**, *58*, 191.

[14] G. J. Fischer, Z. Wang, S.-i. Karato, *Phys. Chem. Miner.* **1993**, *20*, 97.

[15] A. Rockett, C. J. Kiely, *Phys. Rev. B* **1991**, *44*, 1154.

[16] R. Kajimoto, H. Yoshizawa, H. Kawano, H. Kuwahara, Y. Tokura, K. Ohoyama, M. Ohashi, *Phys. Rev. B* **1999**, *60*, 9506.

[17] H. Kuwahara, Y. Tomioka, A. Asamitsu, Y. Moritomo, Y. Tokura, *Science* **1995**, *270*, 961.

[18] M. Nakamura, Y. Ogimoto, H. Tamaru, M. Izumi, K. Miyano, *Appl. Phys. Lett.* **2005**, *86*, 182504.

[19] M. Kasai, H. Kuwahara, Y. Moritomo, Y. Tomioka, Y. Tokura, *Jpn. J. Appl. Phys., Part 2* **1996**, *35*, L489.

[20] W. Prellier, A. Biswas, M. Rajeswari, T. Venkatesan, R. L. Greene, *Appl. Phys. Lett.* **1999**, *75*, 397.

[21] Y. Ogimoto, M. Nakamura, N. Takubo, H. Tamaru, M. Izumi, K. Miyano, *Phys. Rev. B* **2005**, *71*, 060403(R).

[22] Y. Wakabayashi, H. Sawa, N. Takubo, M. Nakamura, Y. Ogimoto, K. Miyano, *J. Phys. Conf. Ser.* **2010**, *211*, 012004.

[23] D. Lu, D. J. Baek, S. S. Hong, L. F. Kourkoutis, Y. Hikita, H. Y. Hwang, *Nature Mater.* **15**, 1255 (2016).

[24] Z. Yu, D. A. Muller, J. Silcox, *J. Appl. Phys.* **2004**, *95*, 3362.

[25] J. Narayan, B. C. Larson, *J. Appl. Phys.* **2005**, *93*, 278.

[26] C. H. Chen, S-W. Cheong, *Phys. Rev. Lett.* **1996**, *76*, 4042.

[27] Y. Wakabayashi, D. Bizen, H. Nakao, Y. Murakami, M. Nakamura, Y. Ogimoto, K. Miyano, H. Sawa, *Phys. Rev. Lett.* **2006**, *96*, 017202.

[28] L. Dong, J. Schnitker, R. W. Smith, D. J. Srolovitz, *J. Appl. Phys.* **1998**, *83*, 217.

[29] T. Ungar, A. Borbely, *Appl. Phys. Lett.* **1996**, *69*, 3173.

Figure Captions

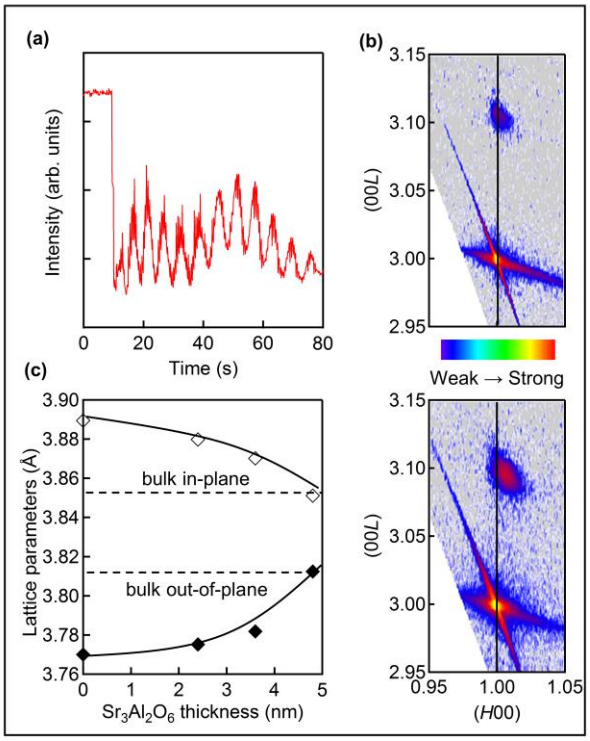

Figure 1. a) RHEED intensity oscillations during $Nd_{0.5}Sr_{0.5}MnO_3$ growth on $Sr_3Al_2O_6$ 3.6 nm / $SrTiO_3$ (001). b) Reciprocal space map of $Nd_{0.5}Sr_{0.5}MnO_3$ 80 nm / $SrTiO_3$ (001) (top) and $Nd_{0.5}Sr_{0.5}MnO_3$ 80 nm / $Sr_3Al_2O_6$ 3.6 nm / $SrTiO_3$ (001) (bottom) at room temperature around the $SrTiO_3$ Bragg peak (103). The solid lines are guides to the eye. The stronger and broader (103) peak for the x = 3.6 film than the x = 0 film is likely due to dislocation confinement in the buffer layer that increases the film crystallinity, and the higher total dislocation density (including those in the buffer layer) from the larger in-plane mismatch broadening the peak.[29] c) $Nd_{0.5}Sr_{0.5}MnO_3$ lattice constants depending on $Sr_3Al_2O_6$ thickness. The dotted lines are bulk in-plane (average of a' and b') and out-of-plane (c') pseudo-cubic lattice constants.

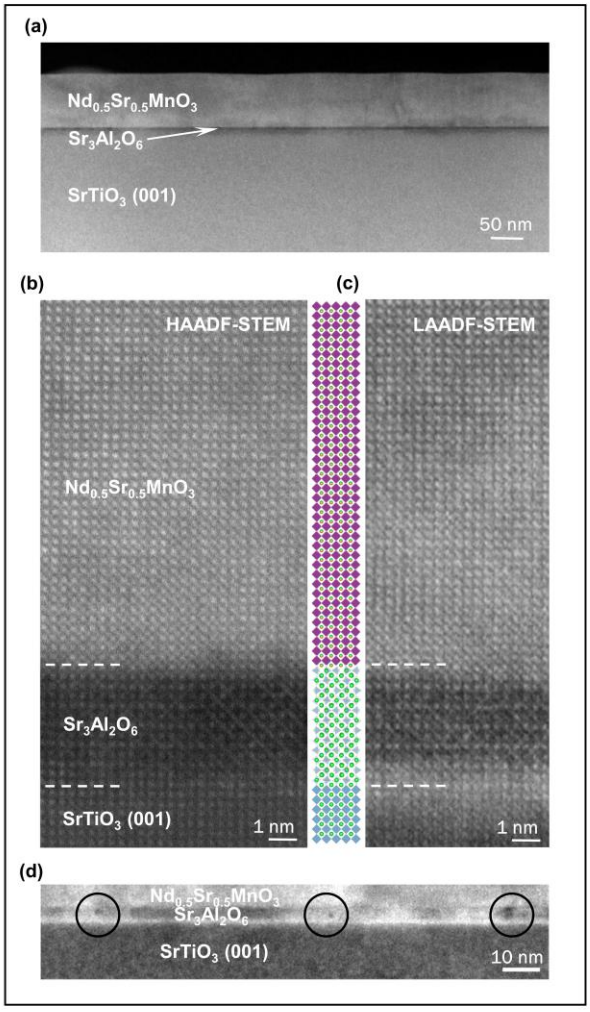

Figure 2. a) HAADF-STEM image of $Nd_{0.5}Sr_{0.5}MnO_3$ 80 nm / $Sr_3Al_2O_6$ 4.8 nm / $SrTiO_3$ (001). b,c) Magnified HAADF-STEM, atomic model (b) and LAADF-STEM (c) images of the same sample. d) LAADF-STEM image around the $Sr_3Al_2O_6/SrTiO_3$ (001) interface showing the misfit dislocations (circled).

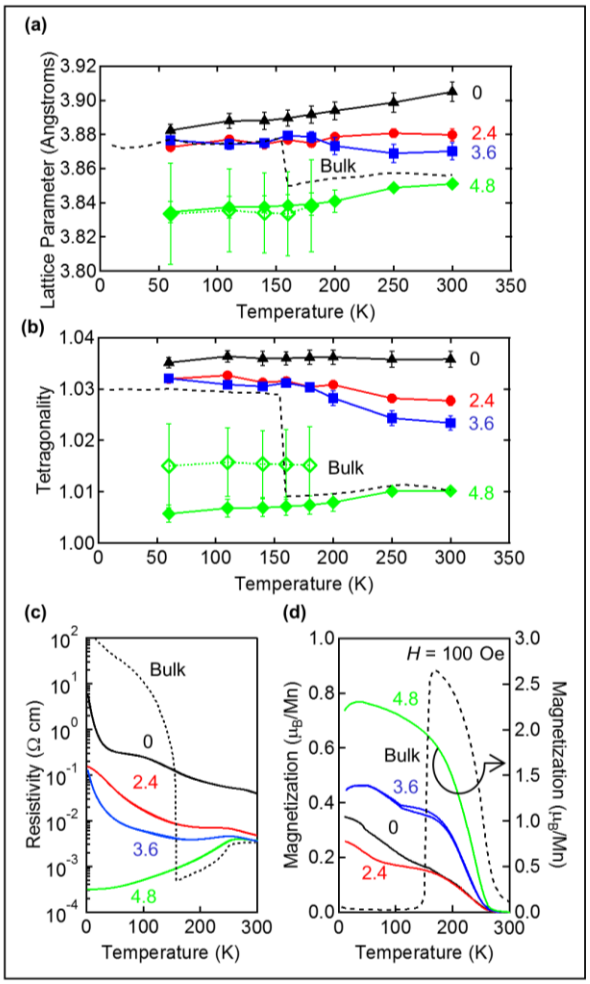

Figure 3. a, b) Temperature dependent in-plane lattice constant a) and tetragonality *c'/a'* b) of $Nd_{0.5}Sr_{0.5}MnO_3$ 80 nm / $Sr_3Al_2O_6$ *x* nm / $SrTiO_3$ (001). Error bars are also shown. The dashed lines indicate the bulk in-plane (average of pseudo-cubic *a'b'*) lattice constant and tetragonality (average of pseudo-cubic *a'b'* / pseudo-cubic *c'*).[17] Filled and empty diamond markers correspond to different domains in *x* = 4.8 film. c, d) Temperature dependent in-plane resistivity (c) and in-plane magnetization (d) curves for $Nd_{0.5}Sr_{0.5}MnO_3$ 80 nm / $Sr_3Al_2O_6$ *x* nm / $SrTiO_3$ (001). The magnetization is measured by warming these samples in 100 Oe external field after cooling in the same field. The values of *x* are marked in the figures. The dashed lines indicate the bulk resistivity and magnetization.[17]

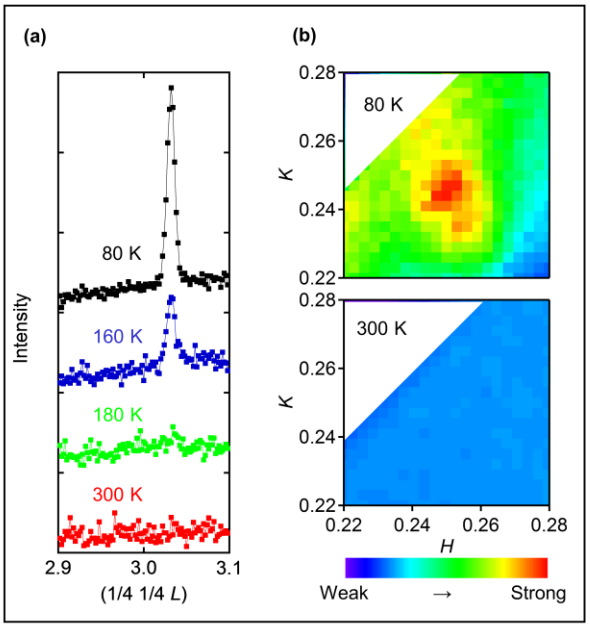

Figure 4. a) *L* scan around (1/4 1/4 3) of $Nd_{0.5}Sr_{0.5}MnO_3$ 80 nm / $Sr_3Al_2O_6$ 3.6 nm / $SrTiO_3$ (001) at different temperatures. b) Reciprocal space mapping around (1/4 1/4 3.03) of $Nd_{0.5}Sr_{0.5}MnO_3$ 80 nm / $Sr_3Al_2O_6$ 3.6 nm / $SrTiO_3$ (001) at 80 K (top) and 300 K (bottom).